



Quantifying Asian and biomass burning sources of mercury using the Hg/CO ratio in pollution plumes observed at the Mount Bachelor observatory

Peter Weiss-Penzias^{a,*}, Dan Jaffe^a, Phil Swartzendruber^{a,1}, William Hafner^a,
Duli Chand^a, Eric Prestbo^b

^a*Interdisciplinary Arts and Sciences Department, University of Washington, Bothell, Bothell, WA, USA*

^b*Frontier Geosciences, Seattle, WA, USA*

Received 26 October 2006; received in revised form 25 January 2007; accepted 26 January 2007

Abstract

Total airborne mercury (TAM) and carbon monoxide (CO) were measured in 22 pollution transport “events” at Mt. Bachelor Observatory (MBO), USA (2.8 km asl) between March 2004 and September 2005. Submicron particulate scattering (σ_{sp}), ozone (O_3), and nitrogen oxides (NO_y) were also measured and enhancement ratios for each chemical and aerosol species with CO were calculated. Events were categorized based on their source regions, which were determined by a combination of back trajectories, satellite fire detections, chemical and aerosol enhancement ratios, and meteorology. The mean $\Delta TAM/\Delta CO$ values for each source region are: East Asian industrial ($0.0046 \pm 0.0013 \text{ ng m}^{-3} \text{ ppbv}^{-1}$, $n = 10$ events, 236 h), Pacific Northwest U.S. (PNW) biomass burning ($0.0013 \pm 0.008 \text{ ng m}^{-3} \text{ ppbv}^{-1}$, $n = 7$ events, 173 h), and Alaska biomass burning ($0.0014 \pm 0.0006 \text{ ng m}^{-3} \text{ ppbv}^{-1}$, $n = 3$ events, 96 h). The $\Delta TAM/\Delta CO$ means from Asian long-range transport (ALRT) and biomass burning events are combined with previous estimates of CO emissions from Chinese anthropogenic, global biomass burning, and global boreal biomass sources in order to estimate the emissions of gaseous elemental mercury (GEM) from these sources. The GEM emissions that we calculate here are: Chinese anthropogenic ($620 \pm 180 \text{ ty}^{-1}$), global biomass burning ($670 \pm 330 \text{ ty}^{-1}$), and global boreal biomass burning ($168 \pm 75 \text{ ty}^{-1}$), with errors estimated from propagating the uncertainty in the mean enhancement ratios and CO emissions. A comparison of our results with published mercury (Hg) emissions inventories reveals that the Chinese GEM emissions from this study are higher by about a factor of two, while our estimate for global biomass burning is consistent with previous studies.

© 2007 Elsevier Ltd. All rights reserved.

Keywords: Mercury; Long-range transport; Emissions; CD; Biomass burning; China

1. Introduction

Mercury (Hg) is a pollutant of global concern due to its ability to bioaccumulate in aquatic systems as methyl mercury, posing health risks to wildlife and humans. Unlike other metals in the atmosphere, Hg largely exists in its elemental form (95–100% Hg^0 or

*Corresponding author. Present address: University of California, Santa Cruz, Department of Environmental Toxicology, Santa Cruz, CA, USA.

E-mail address: pweiss@ucsc.edu (P. Weiss-Penzias).

¹Also at University of Washington, Department of Atmospheric Sciences, Seattle, WA, USA.

gaseous elemental mercury (GEM)), which is rather inert (lifetime = 1/2–2 years) allowing it to be transported globally (Lin and Pehkonen, 1999; Lindqvist et al., 1991; Mason et al., 1994; Schroeder and Munthe, 1998). Reactive gaseous mercury (RGM) and particle-bound (PHg) Hg^{II} compounds make up the remaining fraction of mercury in the atmosphere. These compounds are more water soluble and have an estimated lifetime on the order of several days. GEM + RGM + PHg represent total airborne mercury (TAM).

Primary anthropogenic sources are believed to make up about 30% of all sources of TAM (Bergan et al., 1999; Mason and Sheu, 2002; Selin et al., 2007) and are dominated by coal-fired power plants and other combustion sources, which emit approximately 50–60% GEM, ~30% RGM, and ~10% PHg (Pacyna et al., 2006; Streets et al., 2005). Natural sources are poorly quantified and include the oceans, wetlands, soil, vegetation, volcanoes, and biomass burning. However, it is currently estimated that over two-thirds of the natural source is actually re-emission of previously deposited mercury from anthropogenic origins (Mason et al., 1994; Seigneur et al., 2004; Selin et al., 2007; Strode et al., 2007).

Currently in the United States and elsewhere, there is great interest in assessing the magnitude of anthropogenic and natural Hg sources to the global background (Pacyna et al., 2006) in order to determine the origins of Hg deposited to a particular region (Seigneur et al., 2004; Selin et al., 2007). However, making this assessment involves numerous uncertainties including the GEM oxidation mechanism (Calvert and Lindberg, 2005; Holmes et al., 2006), the anthropogenic emissions inventories (Lin et al., 2006; Ryaboshapko et al., 2004; Slemr et al., 2003) and possible rapid reduction of Hg^{II} to GEM within emission plumes (Lohman et al., 2006). There is also considerable uncertainty associated with the magnitude of re-emission from vegetation, biomass burning, and the oceans (Gbor et al., 2006; Turetsky et al., 2006).

Mercury to carbon monoxide (CO) ratios in pollution plumes from anthropogenic and biomass burning origins have been used previously to constrain the magnitude of Hg sources (Brunke et al., 2001; Friedli et al., 2003a,b; Friedli et al., 2004; Sigler et al., 2003; Jaffe et al., 2005; Slemr et al., 2006). Jaffe et al. (2005) found that the enhancement ratio above the background for $\Delta\text{Hg}^0/\Delta\text{CO}$ was $0.0056 \text{ ng m}^{-3} \text{ ppbv}^{-1}$ at Okinawa, Japan, in six

plumes originating from China. This ratio compares closely to two Asian long-range transport (ALRT) plumes measured in the free troposphere (FT) at Mount Bachelor Observatory (MBO) Oregon, USA ($0.0045\text{--}0.0048 \text{ ng m}^{-3} \text{ ppbv}^{-1}$) (Weiss-Penzias et al., 2006). However, these ratios, along with those measured by Friedli et al. (2004) during the ACE-Asia campaign downwind of Shanghai, suggest that published total Hg anthropogenic emissions inventories for China ($\sim 600 \text{ t y}^{-1}$) are about a factor of two too low (Pacyna et al., 2006; Streets et al., 2005). There are a number of possible explanations for this discrepancy, as outlined by Jaffe et al. (2005).

This current study aims to verify the $\Delta\text{TAM}/\Delta\text{CO}$ ratio in multiple ALRT plumes at MBO and in different seasons in order to more accurately quantify the East Asian Hg source. Additionally, biomass burning is a potentially large Hg source globally (Brunke et al., 2001; Friedli et al., 2001; Cinnirella and Pirrone, 2006; Turetsky et al., 2006), and this study presents emissions estimates based on the results of numerous smoke plume observations from temperate and boreal forests.

2. Methods

2.1. Site description and instrumentation

MBO is located at the summit of a dormant volcano in the Cascade Mountain Range in central Oregon, USA (43.98°N , 121.69°W). At an altitude of 2763 m above mean sea level, the site observes the FT much of the time. A detailed description of the site and a categorization of air mass types during the spring of 2004 has been published previously (Weiss-Penzias et al., 2006). Water vapor mixing ratio measurements at the site have been found to be a good tracer for high altitude FT air (dry, high O_3) or low altitude boundary layer (BL) air (wet, low O_3). The site sees very little influence from regional industrial emissions. FT air masses sometimes contain enhanced levels of pollutants due to ALRT and transport from other regions (e.g. Alaska). RGM concentrations of up to 500 pg m^{-3} have also been observed in FT air during spring and summer, but this is believed to result from in situ production and not long-range transport (Swartzendruber et al., 2006).

Measurements of TAM, CO, O_3 , σ_{sp} , and NO_y , along with ancillary measurements of water vapor,

radon-222, and basic meteorology have been ongoing at MBO since the spring of 2004. The period of measurement in this work is from 28 March 2004 to 30 September 2005. Measurement methods at MBO have been described previously, so only a brief explanation is given here (Swartzendruber et al., 2006; Weiss-Penzias et al., 2006). TAM was measured from March 2004 to March 2005 by converting all Hg species to GEM with a pyrolyzer heated to 500 °C at the inlet, and detecting with a Tekran 2537A cold vapor atomic fluorescence detector. After March 2005 speciated Hg measurements (GEM, RGM and PHg) were made by employing the Tekran 1130 and 1135 speciation units along with the 2537A. The size cut for PHg is estimated to be 2.5 μm (Swartzendruber et al., 2006). TAM for this later time period was obtained by adding together the concentrations of GEM, RGM, and PHg. All measurements were reduced to hourly averages for the present study. CO was measured by a non-dispersive infrared instrument (TECO 48C-TL) and calibrated using a working standard that was referenced to a NIST standard reference gas. O₃ was measured by a standard UV absorbance instrument (Dasibi) and calibrated quarterly with an O₃ transfer standard that was referenced to a State of Washington primary O₃ standard. Submicron σ_{sp} was measured by an integrating nephelometer (Radiance Research), and calibrated quarterly with pure CO₂ gas. The units of scattering are in mega per meter (Mm⁻¹) at standard temperature and pressure. Total reactive nitrogen oxides (NO_y) were measured with a standard chemiluminescence detector (Teledyne-API, 200AU) and calibrated quarterly by diluting a 1 ppmv commercial standard.

2.2. Source region determination during pollution events

We defined pollution events as times when the following criteria were satisfied: (1) CO enhancement of > 15% above the monthly mean for at least 12 h, (2) enhancements in at least one other species (TAM, σ_{sp} , O₃, NO_y), and (3) an ensemble of back trajectories showed a consistent pattern of transport from one of several pre-determined source regions. Details on the last criteria are given below.

Back trajectories were calculated using the Hybrid Single-Particle Lagrangian Integrated Trajectory (HYSPLIT) model (Draxler and Rolph, 2003) with meteorological input from both the National Center

for Environmental Prediction FNL-archive (FNL) and Eta data assimilation system (EDAS) (found online at <http://www.arl.noaa.gov/ready/hysplit4.html>). FNL data is available every 6 h at 1 × 1 degree horizontal resolution with 14 vertical levels. FNL data was used to run trajectories to evaluate long-range transport from Asia and Alaska. EDAS data, with a time resolution of 3 h and a horizontal resolution of 40 km and 27 vertical levels, was used over the continental U.S.

For each hour during an event, 5- or 10-day back trajectories were run from multiple starting locations and altitudes around MBO. Starting locations were spaced at 0.125° latitude and longitude intervals centered on MBO. Altitudes were varied by 200 m intervals from 1300 to 2500 m above the modeled ground level (agl). For each trajectory, residence time as a function of altitude was determined for potential source regions, which were categorized as ALRT, biomass burning Pacific Northwest (BB PNW), biomass burning Alaska (BB Alaska), and U.S. Industrial. These regions are delineated on the trajectory maps in Fig. 1. Note that “source boxes” for fire regions were variable in location. Large numbers of trajectories (> 1000) are calculated for each event (hourly at various starting altitudes) in order to provide a measure of the time spent by an air mass in a source region. The more trajectories calculated, the greater the accuracy in knowing the plume source location (within the inherent uncertainty of the meteorological input data) (Stohl et al., 2003). The timing of the maximum in total trajectory residence time was then compared to the timing of the maximum CO concentration during an event. If there was agreement to within 6 h, the event source region was considered to have been identified. Source boxes for fire regions were determined with the aid of MODIS fire detections from University of Maryland (<http://maps.geog.umd.edu/>).

Enhancements (Δ) for each chemical and aerosol species were determined by subtracting the monthly mean (which is assumed to be representative of background air) (Bertschi et al., 2004), from the highest hourly average during each event.

3. Results and discussion

3.1. Seasonal cycles and lifetimes

Fig. 2 presents the one-week means and standard deviations for NO_y, σ_{sp} , O₃, TAM, and CO over the

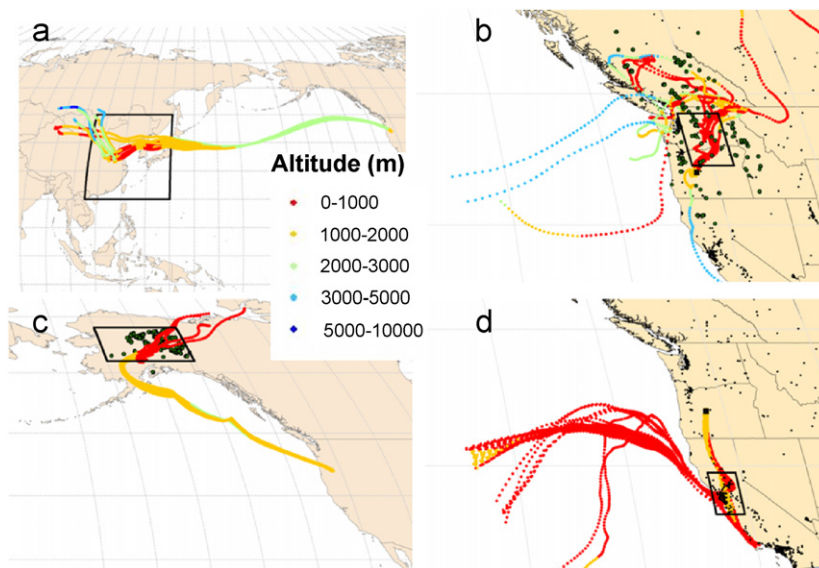


Fig. 1.

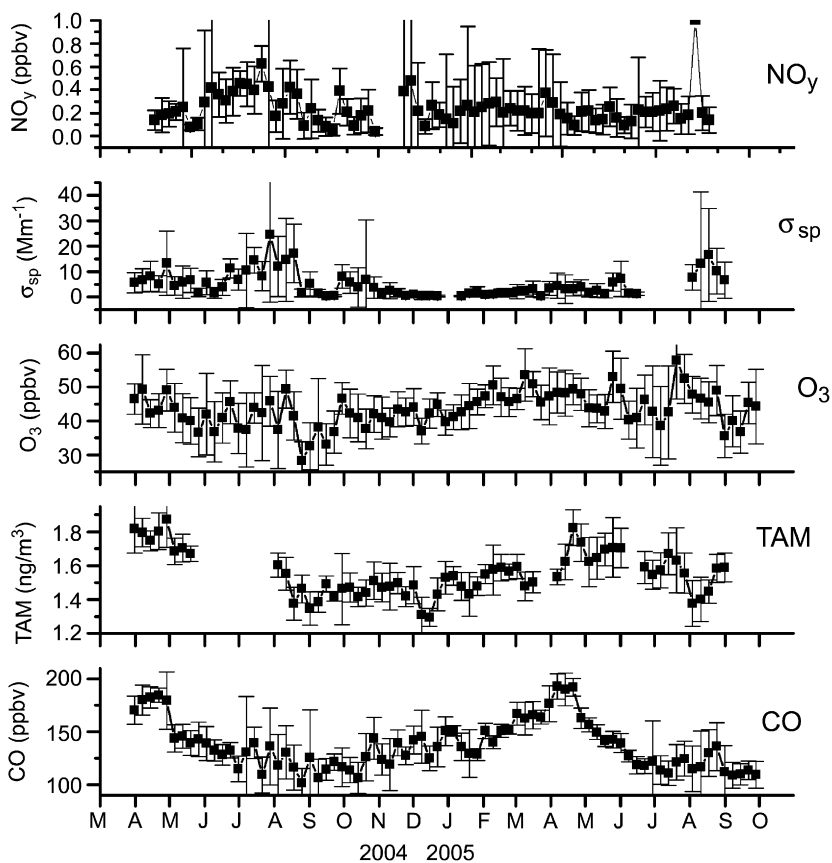


Fig. 2.

period March 2004 to September 2005. TAM displays a slight seasonality, varying from a maximum in April of $\sim 1.8 \text{ ng m}^{-3}$ to a broad fall-winter minimum of $\sim 1.4 \text{ ng m}^{-3}$. The magnitude and timing of this seasonal variation is broadly similar to others measured in northern midlatitude background air (Ebinghaus et al., 2002; Weiss-Penzias et al., 2003). The pronounced springtime maximum of TAM at MBO may reflect the effect of transport from East Asia in the spring—note the similarity with CO. Chemical transport models have shown that Asian industrial emissions account for roughly one-third of the springtime CO concentrations in the Pacific Northwest (PNW) (Liang et al., 2004). Additionally, both the CO and TAM maxima in Fig. 2 are about 10% higher than what was measured at Cheeka Peak (CPO) in the marine boundary layer (Weiss-Penzias et al., 2003), which is consistent with an increase in ALRT with altitude (Liang et al., 2004). The Junge lifetime (Colman et al., 1998) of TAM from the mean and variability from these measurements is 0.51 years, which compares closely to the lifetime of GEM from measurements at CPO in 2001–2002 (0.57 years) (Weiss-Penzias et al., 2003).

3.2. Pollution events—chemical, aerosol, and transport data

From this analysis we have identified a total of 22 pollution events at MBO (Table 1). This section presents the results of the plume detections and has been broken down by the four source regions. Quantitative information for each event, including species enhancements above the monthly mean and the enhancement ratio with CO, is shown in Tables 1a–c. For each source region, we discuss four example pollution events in more detail that describe the range of transport characteristics observed (10 April 2005 (ALRT), 14 August 2004 (BB PNW), 2 September 2004 (BB Alaska), and 7 May 2004 (U.S. Industrial)). Back trajectories for these example events are shown in Fig. 1. A comparison of measured water vapor at MBO with water vapor from regional radiosonde locations at Medford (MFR) and Salem (SLE), Oregon is shown in Fig. 3. Meteorological parameters (and deviation from the monthly mean) for each example event are shown in Table 2. Fig. 4 shows a scatter plot of TAM vs. CO and σ_{sp} vs. CO in order to quantify the differences in ALRT and biomass burning transport.

3.2.1. Asian long-range transport

According to Table 1a, six of the 10 ALRT events occur in the spring and the rest are in the fall, consistent with our understanding of the seasonality of trans-Pacific transport (Newell and Evans, 2000; Weiss-Penzias et al., 2004). ΔCO and ΔO_3 mean values are 58% and 73% higher, respectively, than the mean of 11 ALRT events during 2001–2002 between 0.5 and 4.9 km altitude off the coast of Washington State (Price et al., 2004). This suggests a significant level of interannual variability in the frequency and strength of ALRT. One explanation for the increase in 2004–2005 is that this period is likely to have been influenced by the large Siberian fires during the summer of 2003 (Bertschi and Jaffe, 2005). This allows excess CO to persist into the fall months when its atmospheric lifetime in the northern midlatitudes is longer, thereby causing higher values into the following spring.

$\Delta\sigma_{\text{sp}}$ values show high variability presumably due to the inconsistency of precipitation. ΔNO_y values are zero for six events suggesting that transport times are long compared to the lifetimes of NO and NO₂, and that peroxyacetyl nitrate (PAN) levels are not always enhanced. ΔO_3 values also show high variability due to periodic influences from stratospheric air intrusions (Cooper et al., 2004) and from photochemical loss over the northeastern Pacific Ocean.

TAM and CO are well correlated during every ALRT event with r^2 values >0.5 . $\Delta\text{TAM}/\Delta\text{CO}$ values display the least variability compared to enhancement ratios for the other chemical and aerosol species. The mean value of $0.0046 \text{ ng m}^{-3} \text{ ppbv}^{-1}$ is somewhat lower than (but within 1σ) values obtained in plumes downwind of East Asian sources at Okinawa Island ($0.0056 \text{ ng m}^{-3} \text{ ppbv}^{-1}$) (Jaffe et al., 2005). If this difference is real and not just from the uncertainty in the Hg measurement, it suggests that the lifetime of GEM is shorter than that of CO, which has been suggested for the marine BL (Hedgecock et al., 2005).

Fig. 1a shows nine back trajectories for a typical ALRT event on 10 April 2005 at 11:00 UTC. The transport time from the eastern edge of the Asian box to MBO is approximately 5 days. The source region for this event is the industrialized areas of northeastern China and South Korea where many trajectories descend to $<1000 \text{ m}$ above ground level and have the best chance of picking up pollutants. This trajectory ensemble reveals that an average of 31% of the total trajectory hours was spent in the

Table 1
 (a) Asian long-range transport events observed at MBO during 2004–2005. (b) Biomass burning events. (c) U.S. Industrial events

Date, time of CO peak (local time, PST)	Duration (h)	ACO (ppbv)	Δ TAM (ngm ⁻³)	Δ O ₃ (ppbv)	$\Delta\sigma_{sp}$ (Mm ⁻¹)	Δ NO _y (ppbv)	Δ TAM/ Δ CO (ngm ⁻³ ppbv ⁻¹)	Δ O ₃ / Δ CO (ppbv ppbv ⁻¹)	$\Delta\sigma_{sp}$ / Δ CO (Mm ⁻¹ ppbv ⁻¹)	Δ NO _y / Δ CO (ppbv ppbv ⁻¹)
(a)										
9 April 2004, 12:00	21	37	0.17	18	3.5	0.5	0.0032	-0.06	0.21	0.009
10 April 2004, 15:00	15	40	0.10	28	28	0.5	0.0035	0.00	0.35	0
25 April 2004, 8:00	28	116	0.71	32	57	0	0.0042	0.22	0.49	-0.003
13 May 2004, 8:00	18	56	0.15	31	38	0	0.0048	0.22	0.47	0
23 Oct. 2004, 0:00	26	76	0.22	7.5	0	0.2	0.0026	0.17	0.00	0.004
7 Nov. 2004, 21:00	16	63	0.30	13	3.1	0	0.0044	0.12	0.06	0
14 Nov. 2004, 8:00	19	74	0.38	19	3.7	0	0.0051	-0.02	0.04	0
20 Dec. 2004, 0:00	26	30	0.19	21	0	0	0.0060	0.26	0.00	-0.002
10 April 2005, 5:00	32	55	0.17	15	23	0.3	0.0051	0.21	0.34	0.001
18 April 2005, 6:00	17	21	0.16	4.2	0	0	0.0068	0.25	0.00	-0.001
Mean $\pm 1\sigma$ N = 10 events	22 \pm 6	57 \pm 28	0.26 \pm 0.18	19 \pm 10	16 \pm 20	0.1 \pm 0.2	0.0046 \pm 0.0013	0.14 \pm 0.12	0.20 \pm 0.20	0.0008 \pm 0.003
(b)										
PNW										
14 Aug. 2004, 3:00	19	169	0.31	20	110	0.6	0.0004	0.05	0.61	0.005
17 Aug. 2004, 9:00	32	49	0.05	10	39	0.4	0.0015	0.24	0.53	0.003
20 Aug. 2004, 0:00	46	52	0.04	19	40	0.4	0.0012	0.29	0.57	0.005
14 Oct. 2004, 15:00	18	30	0.07	13	37	0.2	0.0016	-0.02	0.66	0.004
18 Aug. 2005, 13:00	22	62	0.12	4.7	80	0.9	0.0024	-0.02	1.15	0.013
26 Aug 2005, 23:00	18	55	0.19	10	28	0.5	0.0018	0.12	0.72	0.011
27 Aug 2005, 21:00	18	76	0.14	17	40	0.2	0.0010	0.21	0.41	0
Mean $\pm 1\sigma$ N = 7 events	25 \pm 11	70 \pm 46	0.13 \pm 0.10	13 \pm 5.6	53 \pm 30	0.5 \pm 0.3	0.0013 \pm 0.0008	0.12 \pm 0.13	0.66 \pm 0.24	0.006 \pm 0.005
Alaska										
2 Sep. 2004, 23:00	42	186	0.15	8.5	13	0.3	0.0008	0.12	0.05	0.002
2 July 2005, 3:00	27	307	0.43	29	na	1.0	0.0015	0.10	na	0.004
13 Aug. 2005, 22:00	27	66	0.17	7.3	8.1	0.4	0.0020	-0.09	0.15	0.005
Mean $\pm 1\sigma$ N = 3 events	32 \pm 9	186 \pm 121	0.25 \pm 0.16	15 \pm 12	11 \pm 4	0.6 \pm 0.4	0.0014 \pm 0.0006	0.04 \pm 0.12	0.10 \pm 0.07	0.003 \pm 0.002
All biomass burning										
Mean $\pm 1\sigma$ N = 10 events	27 \pm 10	105 \pm 88	0.17 \pm 0.12	14 \pm 7.4	44 \pm 32	0.5 \pm 0.3	0.0014 \pm 0.0006	0.10 \pm 0.12	0.54 \pm 0.32	0.005 \pm 0.004
(c)										
27 April 2004, 2:00	19	19	0.07	8.3	13	0	0.0021	0.02	0.26	0
7 May 2004, 3:00	21	15	0.04	12	13	0	0.00009	0.40	0.44	0
Mean $\pm 1\sigma$ N = 2 events	20 \pm 1.4	17 \pm 3.5	0.06 \pm 0.02	10 \pm 3	13 \pm 0	0	0.0011 \pm 0.0014	0.21 \pm 0.27	0.35 \pm 0.13	0

Bolded enhancement ratio values indicate $r^2 > 0.5$.

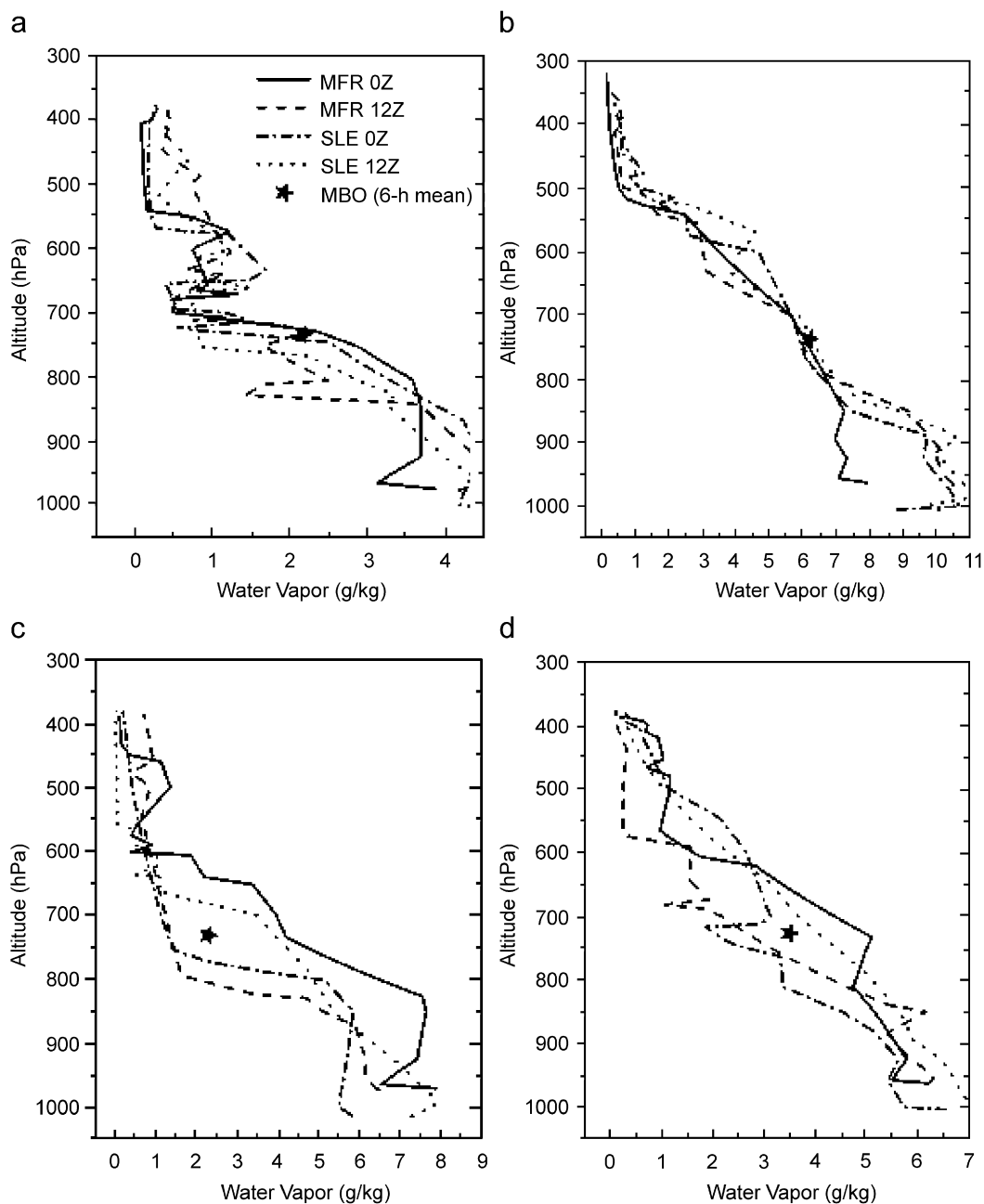


Fig. 3.

East Asian box < 2 km altitude, which is the highest percentage of all ALRT events.

The meteorological conditions at MBO during the 10 April 2005 event are given in Table 2. These show that temperature, water vapor, and wind speed were all well below the monthly nighttime mean. Wind direction was considerably more northerly and pressure was slightly enhanced. These

conditions are all consistent with a high-pressure, subsiding air mass, typical of long-range transport events. Vertical profiles of water vapor from radiosondes are compared with MBO in Fig. 3a. The difference between the 0Z and 12Z soundings gives an indication of the diurnal variability in the height of the BL. This comparison reveals that on 10 April 2005 at 734 hPa, MBO water vapor was

Table 2
Meteorological parameters from four pollution events measured at MBO for the date and hour given

Event source region	Date	Temperature (°C)	Water vapor mixing ratio (g kg ⁻¹)	Wind speed (m s ⁻¹)	Wind direction (deg)	Pressure (hPa)
ALRT	10 Apr. 2005	-8.3 (-2.6)	2.4 (-0.6)	3.7 (-9.1)	331 (+114)	734.3 (+0.8)
BB PNW	14 Aug. 2004	14.1 (+5.7)	5.7 (+0.5)	13.9 (+7.7)	191 (-15)	737.4 (+2.1)
BB Alaska	2 Sep. 2004	-2.8 (-4.9)	2.2 (-1.5)	9.9 (0)	290 (+49)	732.1 (+1.3)
U.S. Industrial	7 May 2004	-2.5 (-0.1)	3.8 (+0.1)	15.2 (+5.0)	194 (-39)	726.4 (-2.0)

Values in parentheses represent the deviation of each parameter from the monthly nighttime mean (20:00–8:00 Pacific Standard Time).

representative of the regional atmosphere and that free tropospheric air masses were likely subsiding down to an altitude of approximately 850 hPa.

3.2.2. Biomass burning (PNW)

A total of seven events from PNW fires were observed during 2004–2005, with all but one event occurring in the summer (Table 1b). These events produced larger ΔCO , $\Delta\sigma_{\text{sp}}$, and ΔNO_y values than the ALRT events due to much shorter transport times from source to receptor, hence less plume dilution, photochemical removal and wet deposition of particles. ΔTAM , on the other hand, is lower compared to ALRT events indicating that a single fire region is a weaker source of mercury than the industrial areas of East Asia. TAM and CO are generally weakly correlated in PNW events, with only one event (18 August 2005) having a correlation coefficient (r^2) > 0.5. The mean $\Delta\text{TAM}/\Delta\text{CO}$ value ($0.0013 \text{ ng m}^{-3} \text{ ppbv}^{-1}$) is more than a factor of three lower compared to ALRT events, with greater variability. $\Delta\text{O}_3/\Delta\text{CO}$ values are quite variable from these fires, and on average are similar to those from ALRT events. σ_{sp} and CO, on the other hand, are well correlated in all PNW biomass burning events, with most r^2 values > 0.8. The mean $\Delta\sigma_{\text{sp}}/\Delta\text{CO}$ value for these events is more than a factor of three larger than that for ALRT events, suggesting that the $\Delta\sigma_{\text{sp}}/\Delta\text{CO}$ is a good indicator of regional biomass burning. $\Delta\text{NO}_y/\Delta\text{CO}$ is also a useful tracer, with a mean value that is almost an order of magnitude larger than for ALRT events.

Fig. 1c shows nine back trajectories for 16:00 UTC on 14 August 2004, the largest regional biomass burning event with $\Delta\text{CO} = 169 \text{ ppbv}$ and $\Delta\sigma_{\text{sp}} = 110 \text{ Mm}^{-1}$. These trajectories indicate that the air mass had considerable contact with active fires at altitudes of < 1000 m for one-half to 3 days

back. Likely fuels in these fires are temperate rain shadow coniferous forests of the northern midlatitudes, with pine, fir and cedar trees dominating.

The meteorological conditions (Table 2) and the water vapor comparison with radiosondes (Fig. 3c) during the 14 August event are consistent with the type of transport shown by the back trajectories. Table 2 shows that there were warm temperatures and high water vapor values accompanied by high wind speed under high pressure conditions. The vertical profiles of water vapor (Fig. 3c) indicate a very large diurnal variation at the surface and good mixing between the BL and the FT until the very low water vapor values that occur at around 500 hPa.

3.2.3. Alaska biomass burning

Three biomass burning events with origins in Alaska were observed during the campaign (Table 1b). Even though these events have relatively long transport times of > 5 days, the ΔCO for these events is quite high, averaging 186 ppbv. This has to do with the size and intensity of these fires compared to the relatively smaller PNW fires, and also the predominance of transport at higher altitudes where CO has a longer lifetime. These fires appear to produce good correlations between TAM and CO, with an average $\Delta\text{TAM}/\Delta\text{CO}$ value of $0.0014 \text{ ng m}^{-3} \text{ ppbv}^{-1}$ which is nearly identical to the mean obtained from regional fires. Thus, we can tentatively conclude that Alaskan boreal forests have the same Hg content as PNW temperate forests. $\Delta\text{O}_3/\Delta\text{CO}$, $\Delta\sigma_{\text{sp}}/\Delta\text{CO}$ and $\Delta\text{NO}_y/\Delta\text{CO}$ values are greatly reduced in Alaskan fires compared to PNW fires due to the effects of transport.

The back trajectories for 8:00 UTC on 2 September 2004 are shown in Fig. 1c. These fires were the largest on record in Alaska (Pfiester et al., 2005) with smoke plumes observed across the

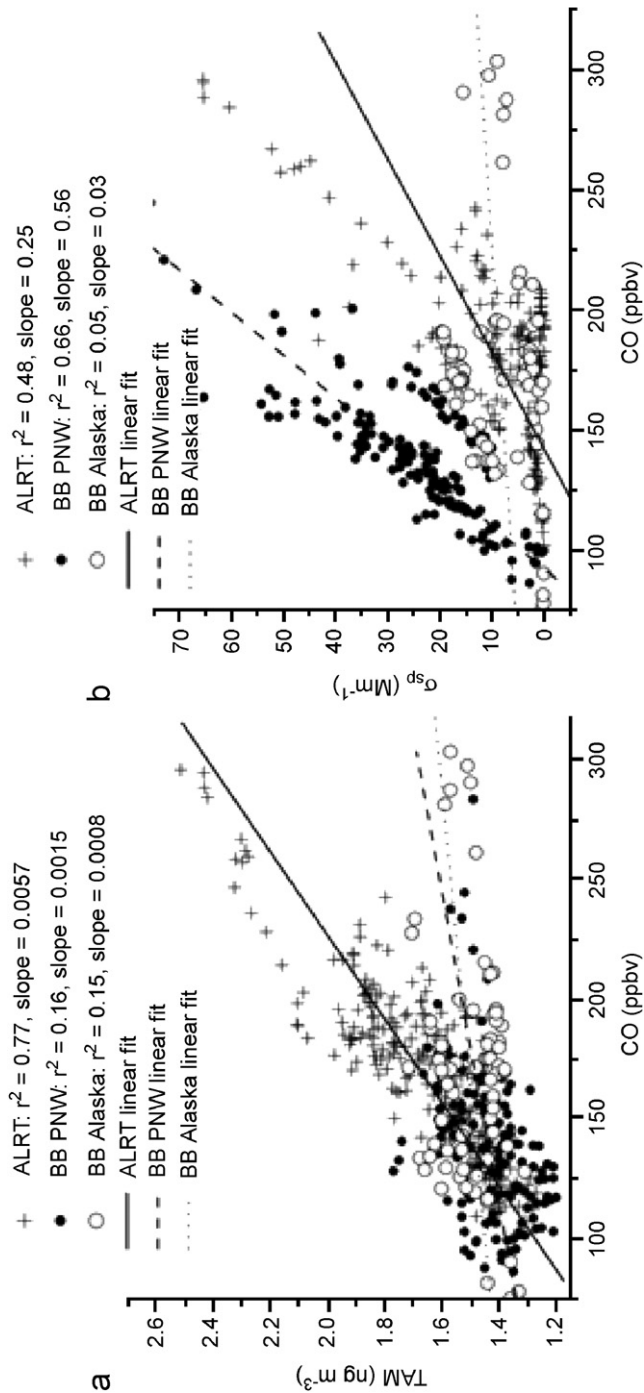


Fig. 4.

northern hemisphere. The trajectories indicate that the air mass stayed relatively stationary for several days at the source region at a low level (<1000 m). Transport to MBO occurred in about seven days, at an altitude of between 1000 and 2000 m, and was likely influenced by clouds and precipitation that were responsible for considerable particle removal.

Meteorological conditions for the arrival time of this event (Table 2) suggest that MBO was sampling in the FT, characterized by low water vapor, cold temperature, and a northerly wind direction. Fig. 3c is consistent with this in showing a pronounced nighttime BL from the surface up to ~825 hPa.

3.2.4. U.S. Industrial

Only two events were observed that could be clearly attributed solely to western U.S. industrial sources during the entire campaign (Fig. 1c, Table 1c). This further underscores the utility of MBO for background air observations. These events produced the smallest ΔCO values of any discussed in this work. However, we can conclude that the mean $\Delta\text{TAM}/\Delta\text{CO}$ from U.S. sources is considerably smaller than from ALRT. $\Delta\sigma_{\text{sp}}/\Delta\text{CO}$ values appear to be larger than those from ALRT, which is consistent with shorter transport times.

3.2.5. Scatter plots of TAM and σ_{sp} vs. CO

Fig. 4 shows scatter plots of TAM and σ_{sp} against CO for all ALRT and biomass burning events. O_3/CO and NO_y/CO scatter plots for all events combined showed little useful characterization information and are not shown. TAM and CO in panel A show a good correlation ($r^2 = 0.77$) and produce a slope that is larger than, but within 1σ of the mean ALRT $\Delta\text{TAM}/\Delta\text{CO}$ in Table 1a. The TAM/CO correlation for biomass burning is rather weak and the slopes are about three to seven times less than ALRT slopes, making TAM a useful tracer for ALRT. The $\sigma_{\text{sp}}/\text{CO}$ relationship in Fig. 4b shows clear differences between source regions, with PNW biomass burning displaying the best correlation and largest slope. Note the non-linear relationship for ALRT events, which likely reflects episodic precipitation scavenging.

3.3. Quantifying mercury emissions

In this section, we derive an estimate for the Hg^0 emission rate from China, world-wide biomass burning, and boreal biomass burning, shown in Table 3. The emission rate is calculated according to

the equation (Jaffe et al., 2005):

$$E_{\text{GEM}} = E_{\text{CO}} \times \Delta\text{TAM}/\Delta\text{CO},$$

where E_{GEM} is the emission rate of elemental mercury (Hg^{II} species are assumed not to undergo transport), E_{CO} is the emission rate of CO, and $\Delta\text{TAM}/\Delta\text{CO}$ is the mean enhancement ratio (Tables 1). Uncertainties are derived according to the equation:

$$\begin{aligned} \% \text{ error } E_{\text{GEM}} \\ = \sqrt{(\% \text{ error } E_{\text{CO}})^2 + (\% \text{ error } \Delta\text{TAM}/\Delta\text{CO})^2}, \end{aligned}$$

where % error is defined as the standard deviation/mean $\times 100\%$.

3.3.1. Chinese emissions

We estimate the GEM emissions from China to be $620 \pm 180 \text{ t y}^{-1}$ assuming CO emissions of $6.00 \times 10^{12} \text{ mol}$ (168 Tg) (Palmer et al., 2003). Our GEM emissions estimate is compared to the “bottom up” emissions inventories from Streets et al. (2005) and Pacyna et al. (2006) for total Hg and GEM. Both inventories include biofuel contributions and assume a constant fraction of Hg species emitted to the atmosphere (53–56% GEM). Similar to the findings of Jaffe et al. (2005), our emissions estimate is more than a factor of two larger than the known GEM emissions from China. This difference is larger than the error in the emissions that we calculated (~30%), and implies a missing or underestimated source. Likely possibilities for missing sources are (Jaffe et al., 2005): (1) underreported point sources, (2) natural geologic sources, (3) re-emission sources from soil and vegetation, and (4) estimated GEM emission fraction in error (i.e. $\geq 56\%$).

3.3.2. Biomass burning sources

Our estimate of $670 \pm 330 \text{ t y}^{-1}$ for GEM emissions from biomass burning (Table 3) assumes CO emissions of $24.6 \times 10^{12} \text{ mol}$ (690 Tg) from Andreae and Merlet (2001). A previous global estimate of Hg emissions from biomass burning (1000 t y^{-1}) was based on measured Hg/CO ratios in smoke plumes from South Africa (Brunke et al., 2001). Alternatively, an emission factor of 71 ng Hg per g of dry matter burned (Friedli et al., 2001), and 8600 Tg y^{-1} dry matter burned globally (Andreae and Merlet, 2001), results in a value of 600 t y^{-1} from global biomass burning.

Table 3
GEM emissions estimates from industrial and biomass burning sources, and a comparison with previously reported values

Emission type	Source region	Measured $\Delta\text{TAM}/\Delta\text{CO}$, this work (mol mol^{-1})	CO emissions, from literature (mol y^{-1})	GEM emissions, this work (metric t y^{-1})	Previously reported Hg emissions (metric t y^{-1})	
					Total Hg	GEM
Anthropogenic industrial	China	5.16×10^{-7} $\pm 1.46 \times 10^{-7}$	6.00×10^{12} $\pm 0.18 \times 10^{12a}$	620 ± 180	536 ^b	300 ^b
					604 ^c	320 ^c
Biomass burning	Global	1.36×10^{-7} $\pm 0.57 \times 10^{-7}$	24.6×10^{12} $\pm 6.1 \times 10^{12d}$	670 ± 330	600 ^{d,e}	–
					1000 ^f	
Biomass burning	Boreal forests	1.36×10^{-7} $\pm 0.57 \times 10^{-7}$	1.07×10^{12} $\pm 0.18 \times 10^{12g}$	29 ± 13 <i>Alaska</i>	22.5 ^h <i>Global boreal</i>	–
				168 ± 75 <i>All boreal forests</i>	53-341 ⁱ	

Global boreal forest + peatland^aPalmer et al. (2003).

^bStreets et al. (2005).

^cPacyna et al. (2006).

^dAndreae and Merlet (2001).

^eFriedli et al. (2001).

^fBrunke et al. (2001).

^gPfister et al. (2005).

^hSigler et al. (2003).

ⁱTuretsky et al. (2006).

Of course, these estimates rely on extrapolations from one experiment in one region to a global value, which is highly uncertain. However, it is evident that biomass burning is a large and naturally variable source that may become more important over time with the warming and drying of certain areas due to climate change. In particular, the boreal forests and tundra regions of the Arctic are highly susceptible to warming and fires, and a recent study has shown that Hg emissions from these regions may have been underestimated by a factor of 10 or more (Turetsky et al., 2006). Therefore, we generated an estimate for the Hg emissions from the Alaska fires of 2004, which burned over 2.5 million ha and were the largest fires on record for Alaska (National Interagency Fire Center, <http://www.nifc.gov/>). CO emissions of 1.07×10^{12} mol (30 Tg) for June–September 2004 from Alaska were obtained from Pfister et al. (2005), based on an inverse model using MOPITT satellite CO observations. Thus, we calculate 29 t y^{-1} for Alaskan biomass burning Hg emissions, which is slightly larger than a previous estimate of boreal forests

globally, based on Hg/CO ratios in smoke plumes (Sigler et al., 2003). If we assume that the area burned in Alaska in 2004 was about 17% of the yearly average global boreal burn area ($15 \text{ million ha y}^{-1}$, Sigler et al., 2003), then we can scale up our estimate to 168 t y^{-1} of Hg for all boreal forests annually. This value falls within a range of values found by Turetsky et al. (2006), which vary by burn intensity, since soil and peat can contain over 20 times more Hg per ha compared to upland forests. Current global models of atmospheric Hg do not contain emissions from biomass burning (Dastoor and Larocque, 2004; Selin et al., 2007), but with more Hg emissions from fires expected in the future due to climate change, this source will no doubt need to be included.

4. Summary

From 28 March 2004 to 30 September 2005, we identified at least 10 plumes of East Asian industrial origin, seven biomass burning plumes from the

PNW, three biomass burning plumes from Alaska, and two plumes of California industrial origin.

Enhancement ratios between TAM, O_3 , σ_{sp} , and NO_y with CO were determined for each event from the slopes of linear regressions. TAM and CO were well correlated in all ALRT events ($r^2 > 0.5$) with a mean slope of $0.0046 \pm 0.0013 \text{ ng m}^{-3} \text{ ppbv}^{-1}$. TAM and CO were less well correlated in biomass burning events and displayed a much lower slope of 0.0013 ± 0.008 and $0.0014 \pm 0.006 \text{ ng m}^{-3} \text{ ppbv}^{-1}$ for PNW and Alaskan fires, respectively. The mean $\Delta\sigma_{sp}/\Delta CO$ for PNW biomass burning was a factor of three larger than that for ALRT events and a factor of six larger than that for Alaska biomass burning events. For PNW biomass burning events, the mean $\Delta NO_y/\Delta CO$ value was at least a factor of two larger than that for other types of events with longer transport times.

Four example events, one from each type (East Asia, PNW biomass burning, Alaska biomass burning, and western U.S. industrial) were presented in more detail in order to identify source regions and transport histories. HYSPLIT back trajectories, local meteorological parameters, and a comparison of MBO water vapor with vertical profiles from regional radiosondes were used to differentiate between events and provide a certain degree of confidence that each event could be attributed to one source region.

Using our observed $\Delta TAM/\Delta CO$ mean values and estimates of the emissions of CO from Chinese anthropogenic, global, and global boreal biomass burning sources, we were able to estimate GEM emissions from each region. We estimate that $620 \pm 180 \text{ ty}^{-1}$ is emitted from China, $670 \pm 330 \text{ ty}^{-1}$ from global biomass burning, and $168 \pm 75 \text{ ty}^{-1}$ from global boreal biomass burning. These emissions comprise a significant portion of all atmospheric Hg sources, currently estimated at 7000 ty^{-1} (Selin et al., 2007). As both Chinese anthropogenic (Wong et al., 2006) and boreal biomass burning (Turetsky et al., 2006) emissions are expected to rise in the future due to economic expansion and warming of the Arctic through climate change, respectively, it is important to continue to monitor pollution plumes from these regions.

Acknowledgments

The authors wish to thank the Mt. Bachelor Ski Area Inc., James B. Dennison, Isaac Bertschi, Carol Higginbotham, Toby Primbs, and Paul Hutter for

field assistance. This work was funded by an EPA STAR Grant (R-82979701). It has not been subjected to any EPA review and does not necessarily reflect the view of the agency.

References

- Andreae, M.O., Merlet, P., 2001. Emission of trace gases and aerosols from biomass burning. *Global Biogeochemical Cycles* 15 (4), 955–966.
- Bergan, T., Gallardo, L., Rodhe, H., 1999. Mercury in the global troposphere: a three-dimensional model study. *Atmospheric Environment* 33, 1575–1585.
- Bertschi, I.T., Jaffe, D.A., 2005. Long-range transport of ozone, carbon monoxide, and aerosols to the NE Pacific troposphere during the summer of 2003: observations of smoke plumes from Asian boreal fires. *Journal of Geophysical Research* 110, D05303.
- Bertschi, I.T., Jaffe, D.A., Jaeglé, L., Price, H.U., Dennison, J.B., 2004. PHOBEA/ITCT 2002 airborne observations of trans-pacific transport of ozone, CO, volatile organic compounds, and aerosols to the northeast Pacific: impacts of Asian anthropogenic and Siberian boreal fire emissions. *Journal of Geophysical Research* 109, D23S12.
- Brunke, E.G., Labuschagne, C., Slemr, F., 2001. Gaseous mercury emissions from a fire in the Cape Peninsula, South Africa, during January 2000. *Geophysical Research Letters* 28 (8), 1483–1486.
- Calvert, J.G., Lindberg, S.E., 2005. Mechanisms of mercury removal by O_3 and OH in the atmosphere. *Atmospheric Environment* 39, 3355–3367.
- Cinnirella, S., Pirrone, N., 2006. Spatial and temporal distributions of mercury emissions from forest fires in Mediterranean region and Russian federation. *Atmospheric Environment* 40, 7346–7361.
- Colman, J.J., Blake, D.R., Rowland, F.S., 1998. Atmospheric residence time of CH_3Br estimated from the Junge spatial variability relation. *Science* 281, 392.
- Cooper, O., et al., 2004. On the life cycle of a stratospheric intrusion and its dispersion into polluted warm conveyor belts. *Journal of Geophysical Research* 109, D23S09.
- Dastoor, A.P., Larocque, Y., 2004. Global circulation of atmospheric mercury: a modeling study. *Atmospheric Environment* 38, 147–161.
- Draxler, R.R., Rolph, G.D., 2003. HYSPLIT (HYbrid Single-Particle Lagrangian Integrated Trajectory). Model access via NOAA ARL READY Website (<http://www.arl.noaa.gov/ready/hysplit4.html>), NOAA Air Resources Laboratory, Silver Spring, MD.
- Ebinghaus, R., Kock, H.H., Coggins, A.M., Spain, T.G., Jennings, S.G., Temme, C., 2002. Long-term measurements of atmospheric mercury at Mace Head, Irish west coast, between 1995 and 2001. *Atmospheric Environment* 36, 5267–5276.
- Friedli, H.R., Radke, L.F., Lu, J.Y., 2001. Mercury in smoke from biomass fires. *Geophysical Research Letters* 28, 3223–3226.
- Friedli, H.R., Radke, L.F., Lu, J.Y., Banic, C.M., Leitch, W.R., Mac Pherson, J.I., 2003a. Mercury emissions from burning of biomass from temperate North American forests: laboratory

- and airborne measurements. *Atmospheric Environment* 37, 253–267.
- Friedli, H.R., Radke, L.F., Prescott, R., Hobbs, P.V., Sinha, P., 2003b. Mercury emissions from the August 2001 wildfires in Washington State and an agricultural waste fire in Oregon and atmospheric mercury budget estimates. *Global Biogeochemical Cycles* 17 (2), 1039.
- Friedli, H.R., Radke, L.F., Prescott, R., Li, P., Woo, J.-H., Carmichael, G.R., 2004. Mercury in the atmosphere around Japan, Korea, and China as observed during the 2001 ACE-Asia field campaign: measurements, distributions, sources, and implications. *Journal of Geophysical Research* 109, D19S25.
- Gbor, P.K., Wen, D., Meng, F., Yang, F., Zhang, B., Sloan, J.J., 2006. Improved model for mercury emissions, transport and deposition. *Atmospheric Environment* 40, 973–983.
- Hedgecock, I.M., Trunfio, G.A., Pirrone, N., Sprovieri, F., 2005. Mercury chemistry in the MBL: Mediterranean case and sensitivity studies using the AMCOTS (Atmospheric Mercury Chemistry over the Sea) model. *Atmospheric Environment* 39, 7217–7230.
- Holmes, C.D., Jacob, D.J., Yang X., 2006. Global lifetime of elemental mercury against oxidation by atomic bromine in the free troposphere. *Geophysical Research Letters* 33, L20808.
- Jaffe, D., Prestbo, E., Swartzendruber, P., Weiss-Penzias, P., Kato, S., Takami, A., Hatakeyama, S., Kajii, Y., 2005. Export of Atmospheric Mercury from Asia. *Atmospheric Environment* 39, 3029–3038.
- Liang, Q., Jaeglé, L., Jaffe, D.A., Weiss-Penzias, P., Heckman, A., Snow, J.A., 2004. Long-range transport of Asian pollution to the northeast Pacific: Seasonal variations and transport pathways of carbon monoxide. *Journal of Geophysical Research* 109, D23S07.
- Lin, C.-J., Pehkonen, S.O., 1999. The chemistry of atmospheric mercury: a review. *Atmospheric Environment* 33, 2067–2079.
- Lin, C.-J., Pongprueksa, P., Lindberg, S.E., Pehkonen, S.O., Byun, D., Jang, C., 2006. Scientific uncertainties in atmospheric mercury models I: model science evaluation. *Atmospheric Environment* 40, 2911–2928.
- Lindqvist, O., Johansson, K., Aastrup, M., Andersson, A., Bringmark, L., Hovsenius, G., Hakanson, L., Iverfeldt, A., Meili, M., Timm, B., 1991. Mercury in the Swedish environment—recent research on causes, consequences and corrective methods. *Water, Air and Soil Pollution* 55, 1–2.
- Lohman, K., Seigneur, C., Edgerton, E., Jansen, J., 2006. Modeling mercury in power plant plumes. *Environmental Science and Technology* 40 (12), 3848–3854.
- Mason, R.P., Sheu, G.R., 2002. Role of the ocean in the global mercury cycle. *Global Biogeochemical Cycles* 16.
- Mason, R.P., Fitzgerald, W.F., Morel, F.M.M., 1994. The biogeochemical cycling of elemental mercury—anthropogenic influences. *Geochimica et Cosmochimica Acta* 58, 3191–3198.
- Newell, R.E., Evans, M.J., 2000. Seasonal changes in pollutant transport to the North Pacific: the relative importance of Asian and European sources. *Geophysical Research Letters* 27 (16), 2509–2512.
- Pacyna, E.G., Pacyna, J.M., Steenhuisen, F., Wilson, S., 2006. Global anthropogenic mercury emission inventory for 2000. *Atmospheric Environment* 40, 4048–4063.
- Palmer, P.I., Jacob, D.J., Jones, D.B.A., Heald, C.L., Yantosca, R.M., Logan, J.A., Sachse, G.W., Streets, D.G., 2003. Inverting for emissions of carbon monoxide from Asia using aircraft observations over the western Pacific. *Journal of Geophysical Research* 108 (D21), 8828.
- Pfister, G., Hess, P.G., Emmons, L.K., Lamarque, J.-F., Wiedinmyer, C., Edwards, D.P., Pétron, G., Gille, J.C., Sachse, G.W., 2005. Quantifying CO emissions from the 2004 Alaskan wildfires using MOPITT CO data. *Geophysical Research Letters* 32, L11809.
- Price, H.U., Jaffe, D.A., Cooper, O.R., Doskey, P.V., 2004. Photochemistry, ozone production, and dilution during long-range transport episodes from Eurasia to the northwest United States. *Journal of Geophysical Research* 109, D23S13.
- Ryaboshapko, A., Artz, R., Bullock, R., Christensen, J., Cohen, M., Dastoor, A., Davignon, D., 2004. Performance of atmospheric long-range transport models for mercury species: results from a model inter-comparison study. *Materials and Geo-environment* 51 (3), 1739–1743.
- Schroeder, W.H., Munthe, J., 1998. Atmospheric mercury—an overview. *Atmospheric Environment* 32, 809–822.
- Seigneur, C., Vijayaraghavan, K., Lohman, K., Karamchandani, P., Scott, C., 2004. Global source attribution for mercury deposition in the United States. *Environmental Science and Technology* 38, 555–569.
- Selin, N.E., Jacob, D.J., Park, R.J., Yantosca, R.M., Strode, S., Jaeglé, L., Jaffe, D., 2007. Chemical cycling and deposition of atmospheric mercury: global constraints from observations. *Journal of Geophysical Research* 112, D02308.
- Sigler, J.M., Lee, X., Munger, W., 2003. Emission of long range transport of gaseous mercury from a large-scale Canadian boreal forest fire. *Environmental Science and Technology* 37, 4343–4347.
- Slemr, F., Brunke, E., Ebinghaus, R., Temme, C., Munthe, J., Wängberg, I., Schroeder, W., Steffen, A., Berg, T., 2003. Worldwide trend of atmospheric mercury since 1977. *Geophysical Research Letters* 30 (10), 1516.
- Slemr, F., Ebinghaus, R., Simmonds, P., Jennings, G., 2006. European emissions of mercury derived from long-term observations at Mace Head, on the Western Irish Coast. *Atmospheric Environment* 40, 6966–6974.
- Stohl, A., Forster, C., Eckhardt, S., Spichtinger, N., Huntrieser, H., Heland, J., Schlager, H., Wilhelm, S., Arnold, F., Cooper, O., 2003. A backward modeling study of intercontinental pollution transport using aircraft measurements. *Journal of Geophysical Research* 108 (D12), 4370.
- Streets, D.G., Hao, J., Wu, Y., Jiang, J., Chan, M., Tian, H., Feng, X., 2005. Anthropogenic mercury emissions in China. *Atmospheric Environment* 39, 7789–7806.
- Strode, S., Jaeglé, L., Selin, N.E., Jacob, D.J., Park, R.J., Yantosca, R.M., Mason, R.P., Slemr, F., 2007. Global Simulation of air–sea exchange of mercury. *Global Biogeochemical Cycles*, in press.
- Swartzendruber, P.C., Jaffe, D.A., Prestbo, E.M., Weiss-Penzias, P., Selin, N.E., Park, R., Jacob, D.J., Strode, S., Jaeglé, L., 2006. Observations of reactive gaseous mercury in the free-troposphere at the Mt. Bachelor Observatory. *Journal of Geophysical Research* 111, D24301.
- Turetsky, M.R., Harden, J.W., Friedli, H.R., Flannigan, M., Payne, N., Crock, J., Radke, L., 2006. Wildfires threaten mercury stocks in northern soils. *Geophysical Research Letters* 33, L16403.
- Weiss-Penzias, P., Jaffe, D.A., McClintick, A., Prestbo, E.M., Landis, M.S., 2003. Gaseous elemental mercury in the marine

- boundary layer: evidence for rapid removal in anthropogenic pollution. *Environmental Science and Technology* 37 (17), 3755–3763.
- Weiss-Penzias, P., Jaffe, D.A., Jaeglé, L., Liang, Q., 2004. Influence of long-range-transported pollution on the annual and diurnal cycles of carbon monoxide and ozone at Cheeka Peak Observatory. *Journal of Geophysical Research* 109, D23S14.
- Weiss-Penzias, P., Jaffe, D.A., Swartzendruber, P., Dennison, J.B., Chand, D., Hafner, W., Prestbo, E., 2006. Observations of Asian air pollution in the free troposphere at Mount Bachelor Observatory during the spring of 2004. *Journal of Geophysical Research* 111, D10304.
- Wong, C.S.C., Duzgoren-Aydin, N.S., Aydin, A., Wong, M.H., 2006. Sources and trends of environmental mercury emissions in Asia. *Science of the Total Environment* 368 (2–3), 649–662.